Study of a New Trigger on Multiplicity and Primary Interaction Vertex using the ALICE Silicon Pixel Detector

F. Antinori [b], R. Caliandro [c], R. Fini [c], F. Formenti [a], V. Lenti [c], F. Meddi [a, e],
K. Šafařík [a], G. Stefanini [a] and T. Virgili [d]

[a] CERN-EP, 1211 Geneva 23, Switzerland
[b] INFN-Padova, I-35131 Padova, Italy
[c] University of Bari and INFN-Bari, I-70126 Bari, Italy
[d] University of Salerno and INFN, I-84100 Salerno, Italy
[e] University of Roma "La Sapienza" and INFN-Roma, I-00185 Roma, Italy

New trigger inputs for the ALICE Central Trigger Processor (CTP) are proposed. They are based on the use of Fast Multiplicity (FM) output signals generated by the ALICE Silicon Pixel Detector (SPD). These can be used for a multiplicity based centrality trigger and for a fast on-line computation of the primary vertex. A simple algorithm for primary vertex location at the trigger level is proposed. The precision that can be achieved with this method on centrality selection and primary vertex location, is discussed for interactions with different pseudo-rapidity density level. The feasibility of background rejection is also considered.

1.   Introduction

The main purpose of this note is to illustrate the basic concepts of a new multiplicity based trigger and the advantages of using the information provided by the ALICE Silicon Pixel Detector (SPD) [1,2] at trigger level. We propose to use the information extracted from a single layer of the ALICE SPD to compute: 1) the total multiplicity (MLT) of the event, and 2) the primary vertex position along the Z-axis (Z_v). In addition we apply a correction to the multiplicity threshold to generate the trigger selection according to the actual measured Z_v value.

We first give a short overview of the ALICE trigger system, the ALICE SPD and the SPD readout system including the Fast Multiplicity signal characteristics. A realistic estimate of the performance of the proposed trigger based on a detailed simulation of the apparatus is presented with a systematic study of the event by event fluctuations. Trigger design specifications and a possible implementation scheme are also reported. Finally, some preliminary considerations on the background rejection are presented.

2.1   ALICE trigger

The ALICE trigger [3] is organised in 3 levels: Level0 (L0), Level1 (L1) and Level2 (L2), with fixed time latencies. The Central Trigger Processor (CTP) delivers the corresponding signals to the ALICE detectors and receives from them the trigger inputs and the BUSY signal. The trigger detector information is used by the CTP to produce a trigger decision for each LHC bunch crossing, i.e. every 25 ns in p-p mode and every 125 ns in ion-ion mode.

The trigger inputs delivered to the CTP are grouped according to their latencies. At L0 only those signals transmitted to the CTP electronics within 900 ns can contribute. All other trigger contributions, too late for L0 and sent to the CTP within 5.8 μs, are used at L1.

L0 provides the earliest strobe to the Front-End (FE) electronics of some detectors. These detectors use a FE based on a 'sample and hold' electronics, which needs to start the conversion process at 1.2 μs after the interaction time. In order to achieve this goal the fastest copper coaxial cables are used to transmit this trigger signal.

L1 uses all the available information from the trigger detectors and allows a rejection of the trigger classes, at 6.5 μs. At L1 detector data are strobed into a Multi-Event Buffer (MEB) in the FE electronics. This allows for a better use of the bandwidth between the detectors and the DAQ where optical links are used and reduces, at the same time, the number of these connections.

The L2 trigger waits for the end of the Time Projection Chamber (TPC) sensitive period, in order to reject events that could not be reconstructed because of pile-up in this detector. This level arrives 88 μs after the interaction time and is necessary to provide "past future protection" against the non negligible probability of multiple interactions occurring during the TPC drift time.

L1 and L2 trigger signals are delivered using the RD12 Trigger Timing and Control System (TTC) [4].

A fourth level (Level3), based on more complex computations using a PC farm, which should produce partial online reconstruction of events and online filtering, is being considered.

2.2   ALICE SPD overview

The SPD consists of the two innermost layers of the ALICE Inner Tracking System (ITS) [1,5], in a barrel geometry. Pixel detectors allow real 2D position measurements, which facilitate pattern recognition and vertex reconstruction at high track densities.

The SPD is mainly designed to reconstruct primary and secondary vertices for general tracking, dimuon physics and for Charm and Beauty studies. Its impact parameter resolution is $\sigma(r\phi) \approx 50$ μm at P_T ≈1 GeV/c and its primary vertex resolution is of the order of some tens of microns in the case of Pb-Pb collisions. It features a high granularity cell size (50 x 425 μm^2), in order to cope with particle densities up

to 90/cm^2, corresponding to ≈8000 tracks per unit of pseudo-rapidity. In these conditions, in fact, the average occupancy is lower than 3%.

As is generally the case in the LHC experiments, the SPD is based on hybrid silicon pixel detector assemblies, in which readout chips are bump-bonded to silicon sensors [6]. The ALICE SPD front-end electronics is all implemented in state-of-the-art CMOS 0.25 μm technology, using radiation hardening design rules [7,8]. This allows obtaining low power consumption, low threshold and good radiation hardness.

The ALICE SPD basic building block is a 'ladder', composed by 5 readout chips bump bonded to a single silicon sensor. Two ladders are aligned in Z (i.e. are parallel to the colliding beams direction) to form a 'half stave'. Each ladder is 12.80 mm wide and 70.72 mm long.

The SPD consists of two cylindrical layers (Fig. 1a), each subdivided into ten sectors in the rϕ-plane, at r = 4 cm and r = 7 cm, respectively, from to the beam axis. Each sector consists of two staves for the inner layer and of four staves for the outer layer, which features a turbine blade-like layout (Fig. 1b). The total number of half-staves is 40 for the inner layer and 80 for the outer layer, giving a total of 240 ladders, 1200 chips and ≈ 10^7 pixel channels.

For interactions located at the centre of the SPD, the pseudo-rapidity (η) coverage is −1.98< η <1.98 for the inner layer and −1.46< η <1.46 for the outer layer. For those interactions that are displaced along the Z-axis respect to the centre of the SPD, the η coverage range will depend on the actual primary position inside the interaction diamond. The primary vertex distribution is characterised by a σ ≈ 5.3cm along the Z-axis and of few tens of micrometers along the transverse plane.

Further information on the SPD can be found in the ITS Technical Design Report [1] and in the most recent general review [5,9].

2.3   ALICE SPD readout and Fast Multiplicity signal

The basic readout unit is a half stave. The data flow in each half-stave is supervised by a control chip (Pilot) mounted at the edge of the half-stave. The Pilot chip incorporates a state machine which strobes the data transfer in the pixel chip to the MEB (four events), on receipt of a L1 from the CTP. The Pilot also handles the multiplexing of output data from the readout chips and the downloading of the chip parameters. At the nominal frequency of the readout clock (10 MHz), the SPD is read out in 256 μs. Data transfer is initiated by a positive L2 trigger decision. In addition to the normal binary output data, each readout chip also generates an analogue Fast Multiplicity signal via a current like output stage. This signal has the time duration of a half clock period and amplitude proportional to the number of pixel cells that fired inside the chip. The current signals from all the chips on a half-stave are combined on the pixel bus and provide a current pulse synchronous with the 10 MHz read-out clock. The masking facility of the individual cell in the pixel chip is effective not only for normal data read-out but also for the Fast Multiplicity output, so this output is not affected by noisy pixels.

Detailed descriptions of the front-end and readout electronics are found in [1,10,11].

3.   Total multiplicity and primary vertex determination

We propose to compute the total multiplicity (MLT) and the primary vertex position along the Z-axis (Z_v), determining separately the multiplicity for each half-layer, i.e. for the right and left part of one SPD layer. This multiplicity information can be obtained on-line using the Fast Multiplicity output present in each read-out chip as described in the previous paragraph. The total multiplicity is proportional to the sum of the left and right contributions, whereas the left-right asymmetry can be used to compute the vertex position. Our approach does not require the correlation between SPD layers in order to get a good precision in a short time.

Using simple considerations on acceptance, we see that as the vertex moves along the Z-axis, the pseudo-rapidity acceptance changes. As a consequence, the number of particles detected in the two halves of one layer varies. In Fig. 2a and in Fig. 2b we show the η-acceptance as a function of Z_v for the inner and

the outer layer, respectively. In each figure three curves are plotted, referring to the two extreme points and to the middle one of each layer. The same behaviour is evident in both figures, but is more marked for the inner layer. This is true for each half-layer η-acceptance and for the total η-acceptance in a layer. The η distribution is expected to be symmetric with respect to $\eta=0$ in the SPD η acceptance region. As a consequence, the variations in the η-acceptance for each half-layer with respect to the layer central region, due to different vertex positions, give rise to a difference in the measured multiplicity. The effect on the measured multiplicity is ~3% for a vertex at $Z_v = \pm 5$ cm, it becomes ~15% for vertex at $Z_v = \pm 10$ cm and ~ 40% for vertex at $Z_v = \pm 15$ cm. This fact implies that, for the same centrality level, interactions with different Z_v values will present different multiplicity. It is possible to correct for this effect taking into account the actual vertex position, which can be calculated online using a hardware processor. In this way, it is possible to recompute the multiplicity threshold so as to apply it to the event, taking into account its Z_v value. This correction allows a good uniformity in the multiplicity trigger as Z_v moves from the centre to the sides of the interaction vertex diamond, keeping the precision of the cut at ~ 1%. It would otherwise deviate by ~ 10% for $Z_v = \pm 10$ cm.

4.   Monte Carlo simulation

In order to have a realistic estimate of the performance of the proposed trigger a detailed simulation of the SPD is needed. This can be done in the framework of AliRoot [12], the standard ALICE simulation and analysis package. We note that in the first layer the staves are almost perpendicular to the radial direction, while in the second layer they are tilted (turbo layout) in order to ensure that no particle can go undetected through the openings among the staves above a momentum cut off of about 27 MeV/c. This simulation of the detailed pixel response is crucial in order to determine the number of fired pixels.

The model to simulate the response of pixel detectors has been already presented [13] and its capability to simulate the SPD layers in AliRoot has been described in [14].

The AliRoot Monte Carlo performs event generation and particle tracking in the experimental apparatus. It simulates the δ-ray production and the energy loss in the detector and its output consists of a set of hits produced by charged particles. The information stored for each hit consists of the coordinates, the track label, the track status, the energy lost by the charged particle and its momentum at the hit position. This information is then used in the simulation to create the digits, namely the pixels fired in the two layers of the SPDs, using the model described in [14].

The basic element of the model is a geometrical description of the pixel structure; the pixel cells are contiguous and the energy loss is deposited proportionally to the length of the track in each cell. In order to determine if a pixel is fired or not, a software threshold E_t is applied to the energy lost E_l in a single cell.

The noise and the spatial dispersion of the thresholds are simulated by introducing a pedestal E_p, which fluctuates from event to event and from pixel to pixel with a Gaussian distribution centred at zero with a standard deviation σ. A pixel is then fired if $E_p + E_l$ is greater than E_t. The σ parameter is interpreted as the square root of the variance of the distribution describing the threshold dispersion in space and the variance of the distribution describing the pedestal fluctuation in time, due to noise.

Coupling effects can be also accounted for in the model. Two parameters F_r and F_c are introduced in the model to represent the fraction of the energy E_l lost in a cell that is assigned to the two nearest cells in respectively row and column direction. Accordingly the energy fraction assigned to the two next cells is respectively F_r^2 and F_c^2 and so on (see [14] for details).

4.1 Results

For the present study AliRoot v.3.04 was used. We generated particles with the AliRoot internal HIJING parametrisation in the range $10° < \theta < 170°$ for the polar angle and with full azimuthal angle coverage. Several event samples were generated with different values for the number of charged particles per unit of pseudorapidity (η) at central η ranging from 200 to 8000.

Particles were traced through the ITS using GEANT 3.21 with all the physical effects switched on, including δ-ray production, with the threshold set to E_δ = 70 keV. The beam pipe and the magnetic field were also switched on in all the simulations.

The parameters used in the detailed simulation were adapted to the foreseen characteristics of the new ALICE1 chip [2,9] and set to the following nominal values [1]:

E_t = 7.2 keV (2000 e⁻);

σ = 1 keV (280 e⁻);

F_r = 0, F_c = 0.

Let N_l and N_r be the number of digits respectively in the left and right side of the layer. This is the information coming from SPD, which can be used in the proposed trigger through the quantities $N_l + N_r$, the measured multiplicity, and $(N_l - N_r)/ (N_l + N_r)$, the left-right asymmetry. The aim of this study is to correlate these quantities to the true event multiplicity (MLT) and to the Z position of the primary vertex along the beam axis (Z_v). The other two vertex coodinate are fixed to X_v =0 and Y_v =0.

In Fig. 3a the correlations between the generated multiplicity and the total number of produced digits are reported for both layers, in the case of the event vertex position fixed at Z_v =0. The generated multiplicity can be measured by the dn/dη, i.e. with the number of charged particles in the central unit of eta, and in the following we will consider MLT ≡ dN/dη. In both layers the trend is linear in the considered multiplicity range and these curves can be used to calibrate the multiplicity trigger.

The correlation between the left-right asymmetry and the longitudinal position of the vertex for both layers is shown in Fig. 3b, using the value dn/dη ~ 4000. A clear correlation is shown which is steeper for layer 1 than for layer 2. The calibration of the primary vertex trigger can be done by means of these curves.

4.2   Study of the fluctuations

In the plots of Fig. 3a and Fig. 3b the statistical errors on $N_l + N_r$ and $(N_l - N_r)/ (N_l + N_r)$ are included. They are negligible for the present study. However, the fluctuation of the measured quantities from event to event with the same multiplicity and primary vertex position is not negligible and needs to be investigated. For this purpose, we generated a set of 15 events for each of the above described conditions. The spread of the correlation between the total number of digits and the multiplicity can be seen in Fig. 4a, where the results from all the generated events are plotted together. The spread of the correlation between the left-right asymmetry and Z_v is shown in Fig. 4b. In the simulations, the true event multiplicity and the primary vertex position are fixed and the observed fluctuations in the number of digits reflect the effects of the tracking and the SPD response. In order to estimate the fluctuations on the variables MLT and Z_v we fit the plots shown in Fig. 4a and Fig. 4b with a straight line of the form:

y= a * x + b

Where

y = ($N_l + N_r$)   and   x = (dn/dη)$_{max}$ for Fig. 4a

y = (Nl - N_r)/(Nl + N_r)   and   x = Z_v for Fig. 4b.

We invert the functions and propagate the errors of the measured variables $N_l + N_r$ and $(N_l - N_r)/(N_l + N_r)$ on the variables MLT and Z_v, respectively, taking into account the errors in the determination of the two coefficients. The errors on the N_l ad N_r are assumed to be of the order of the square root of N_l and N_r, respectively. For Z_v the limited range | Z_v | < 5cm was considered in the fit, to exclude the region where the correlation is no more a straight line (see Fig. 4b). The results of this procedure are shown in Fig. 5a and Fig. 5b, respectively. In Fig. 5a the relative error on dn/dη, that is the relative error on MLT, is shown as a function of the generated pseudo-rapidity density. In Fig. 5b the absolute error on Z_v is shown as a function of the primary vertex position used in the generation.

It can be seen that the relative error on the multiplicity is less than 2% up to a lower multiplicity values (dn/dη~1000) for both layers. It is less than 1% for dn/dη > 3500.

The error on the primary vertex position is lower for lower values of $|Z_v|$. The average value of the error in the considered Z_v range ($|Z_v| < 5$cm) is 3.2 mm for layer 1 and 4.2 mm for layer 2.

It is worthwhile noticing that the inner SPD layer has, as expected, a lower error in the primary vertex determination, while the two layers are almost equivalent in the multiplicity determination. Similar results could be obtained if a larger eta range would be considered. This is due to the fact that at this multiplicity the larger coverage of layer 1 will not give more information on the centrality, provided that the eta distribution is smooth and the statistic is enough. Moreover, the turbo geometry in layer 2 enhances the number of fired pixels related to each track, and then the sensitivity of the detector. This effect is partially equilibrated by the background produced in the inner SPD layer, resulting in a global equivalence of the two layers.

4.3   Correlation of the multiplicity and primary vertex information

One of the advantages of the proposed trigger is the possibility to correlate the information on the measured multiplicity with that on the left-right asymmetry. This allows a better definition of the trigger thresholds, and therefore the selection of central events is improved.

In Fig. 6a the measured multiplicity $N_l + N_r$ of both layers is correlated to the primary vertex position. For each vertex position, the results from 15 events generated in the same conditions are shown. The generated multiplicity was fixed to dn/dη=4000. A decrease in multiplicity is noticed for interactions with $|Z_v| > 5$cm and this can be accounted for in the tuning of the multiplicity trigger. The measured left-right asymmetry does not depend on the generated multiplicity, as shown in Fig. 6b for both layers, where the vertex position was fixed at $Z_v = 0$ in all the simulations. Nevertheless, it can be noted that at low multiplicity the fluctuation on the asymmetry are not negligible, and therefore the thresholds on the primary vertex trigger should have a larger tolerance at smaller multiplicity values.

5.   Background rejection

The pseudorapidity distribution for particles produced in beam-gas interactions, namely p-O at 7 TeV p beam and Pb-O at 2.8 TeV per nucleon Pb beam, can be parameterised by Gaussians, centred at |η|=4.68 and |η|=5.26, respectively. The normalisation factors and the standard deviations for such Gaussian distributions are respectively, 4.43 and 2.54 for p-O, 4.27 and 2.16 for Pb-O. The secondary particles produced by these interactions could arise from the two 20m straight-line beam-transport sections, located before and after the ALICE interaction point. The covered η range is reduced and displaced toward higher pseudorapidity values. For instance, in case of a background interaction located at 10m from the centre of the ALICE apparatus, we obtain an average η measured by the SPD of 6, and for the accepted η range a value of 0.03. As a consequence, the total primary tracks in the acceptance of each pixel layer are less than ≈50 in case of Pb-O interaction, and less than ≈6 in case of p-O interaction.

The number of secondary particles produced in the beam pipe is much lower for background interactions produced at $|Z_v|$<15cm than for those produced very far from the SPD centre. In fact, the material thickness to be traversed is limited to 10% and 20% of radiation length for the angles seen by the inner and the outer pixel layer. These numbers could be a factor 10 higher in case of beam-gas interactions located at 20m. To summarise, both SPD layers are almost insensitive to multiplicity background due to single beam-gas interactions, especially those located at $|Z_v|$<15cm. Nevertheless, to complete the study is still missing a complete Monte Carlo simulation that takes into account the effects due to the materials encountered on the beams transport line by the beam-gas interaction secondary particles.

6.   FM trigger design considerations

The dynamic range requirements can be derived from the highest multiplicities occurring in a single pixel chip and in a half stave, respectively, for the most central Pb-Pb events, with $(dn/d\eta)_{max}$ =8000.

We find that, for these events, the highest multiplicity in a single chip corresponds to 210 and 115 hits, for the inner and outer layer, respectively, that is approximately equivalent to twice the mean value from a half-stave. This occurs for the chips located at Z_v values nearest to the interaction point. For the same events the lowest multiplicity value for a single chip is found to be 40 and 25 for the two layers, corresponding to $\approx$ 20% of the mean value for the chips in a half-stave. This corresponds to chips with Z values most far from the primary vertex and is valid for Z_v =0. In these conditions we require an uncertainty of less than 10% on the single chip multiplicity range, corresponding approximately to the minimal statistical fluctuations. On the other hand, preliminary measurements on a single chip and in ideal laboratory environment, have already shown a level of clock synchronous noise, in the FM signal, with amplitude fluctuations of approximately 5 hits for one chip. This could perhaps be improved by using optimal filtering techniques.

In general, prompt on-detector digitisation of the FM signal would yield the best results. The converted FM data would be transmitted over the 800Mb/s serialiser/divider optical fibre link used for normal readout data transfer. The bandwidth of the link would be adequate. The ADC should have a conversion time less than 100ns.

A fast 10-bit linear ADC would allow to achieve the objective. However there is no readily available commercial low-power IC with these specifications; the development of a dedicated ASIC would raise formidable challenges, particularly on account of the time schedule and the very demanding constraints in space, power dissipation and radiation levels.

The less ambitious goal of an 8-bit equivalent resolution might lead to more realistic implementation perspectives. However this would place some limitation to the detection of events with particularly low multiplicity. Some improvement might be obtained by using a non-linear transfer function with a controlled compression of the signals on the upper part of the range. On-detector digitisation would still require the development of a dedicated low-power flash ADC ASIC.

One potential problem of on-detector digitisation would be the latency deriving from serialisation and transmission. A preliminary estimate shows that this can be solved but at some price in complexity.

However if an 8-bit equivalent resolution turns out to be adequate, an alternative method would consist in the analog transmission of the FM signal over optical fibres to a processor outside the detector. It has already been demonstrated [15] that the required dynamic range can be obtained with laser diode transmitters.

In conclusion, the choice of the technique will eventually be determined by various constraints:

- Space available for on-detector electronics, particularly in the case of the inner layer. This is severely limited to a few mm^2 in footprint and about 1 mm in height;

- Additional power dissipation load to the cooling system. The added heat sources are not distributed along the Z-axis, but localised at the end of each half-stave.

- Signal integrity and noise reduction;

- Signal processing time and transmission delay, in case that one of the aims were to contribute to L0 trigger ($\approx$900ns latency).

To determine the most realistic choice, it is necessary to extend the study of the Fast Multiplicity signal, so far limited to a single chip, to a prototype of a real half-stave. This is the objective of the work in the next few months.

7.   Conclusion

We illustrate the possibility to provide additional inputs to the ALICE trigger, based on the SPD. These trigger inputs can be used for centrality selection and primary vertex determination along the Z-axis. A simple and fast algorithm for Z_v calculation was presented.

We show that the measured Z_v position could be used in order to improve the precision in the determination of the centrality selection, due to the finite dimension of the interaction diamond.

Detailed Monte Carlo simulations of the proposed trigger performance have been done, taking into account event-by-event fluctuations.

The combined use of both multiplicity and vertex position information could also help in beam-gas rejection. This appears feasible for vertices located inside the interaction diamond ($|Z_v|<15$ cm).

Design considerations concerning the dynamic range and the required precision accuracy have been given.

The main objectives of the ongoing study have been outlined.

Acknowledgements

References

[1]   ALICE-T.D.R., "Inner Tracking System", CERN/LHCC 99-12, ALICE TDR 4.

[2]   W. Snoeys et al., "Pixel readout electronics development for ALICE PIXEL VERTEX and LHCb RICH", Paper presented at PIXEL 2000, Genova, Italy, June 5th-8th, 2000.

[3]   O. Villalobos Baillie et al., "The ALICE central trigger processor", Presented at 6-th Workshop of Electronics for LHC Experiments, Cracow, Poland, 11-15 September 2000.

[4]   See web site: http://www.cern.ch/TTC/intro.html.

[5]   F. Meddi, "The ALICE Silicon Pixel Detector (SPD)", Invited talk presented at PIXEL 2000, Genova, Italy, June 5th-8th, 2000.

        See web sites: http://alice1.web.cern.ch/alice1/, http://www.pd.infn.it/spd/.

[6]   J. H. Lau, "Flip-chip Technologies", Mc Graw-Hill (1995).

        S. Cihangir and S. Kwan, "Characterization of Indium and Solder Bump Bonding for Pixel Detectors", Paper presented at the 3rd International Conference on Radiation Effects on Semiconductor Materials, Detectors and Devices, Florence, Italy, June 28-29, 2000.

[7]   F. Faccio et al., "Total dose and single event effect (SEE) in a 0,25 μm CMOS technology", LEB98, INFN Rome, 21-25 September 1998, CERN/LHCC/98-36, October 30, 1998, 105-113.

W. Snoeys et al., "Layout techniques to enhance the radiation tolerance of standard CMOS technologies demonstrated on a pixel detector readout chip", 8-th European Symposium on Semiconductor Detectors Schloss Elman, June 14-17, 1998.

[8]   J. J. van Hunen et al., "Irradiation and SPS Beam Tests of the ALICE1LHCb Pixel Chip", Paper presented at LEB 2001, 7th Workshop on Electronics for LHC Experiment, Stockholm, Sweden, 10-14 September 2001.

[9]   G. Anelli et al., "Recent results from the ALICE Silicon Pixel detector", Paper presented at VERTEX 2001, 10th International Workshop on Vertex Detectors, 23-28 September in Brunner, Switzerland.

[10]   G.Anelli et al., "The Alice on-detector pixel PILOT system-OPS", Paper presented at LEB 2001, 7th Workshop on Electronics for LHC Experiment, Stockholm, Sweden, 10-14 September 2001.

[11]   F. Antinori et al, "The ALICE Pixel Detector readout Chip Test System", Paper presented at LEB 2001, 7th Workshop on Electronics for LHC Experiment, Stockholm, Sweden, 10-14 September 2001.

[12]   See web site: http://www1.cern.ch/ALICE/Projects/offline/aliroot/Welcome.html/.

[13]   R. Caliandro et al., ALICE internal note INT-01-05, February 2001.

[14]   R. Caliandro et al., ALICE internal note INT-00-23, September 2000.

[15]   G. Hall, "Analogue optical data transfer for the CMS tracker", Nucl. Instr. And Meth. in Phys. Res. A 386 (1997) 138-142.

F.Vasey et al., "project status of the CMS tracker optical links", Presented at 6-th Workshop of electronics for LHC Experiments, Cracow, Poland, 11-15 September 2000.

See web site: http://cms-opto.web.cern.ch/cms-tk-opto/wdocs/.
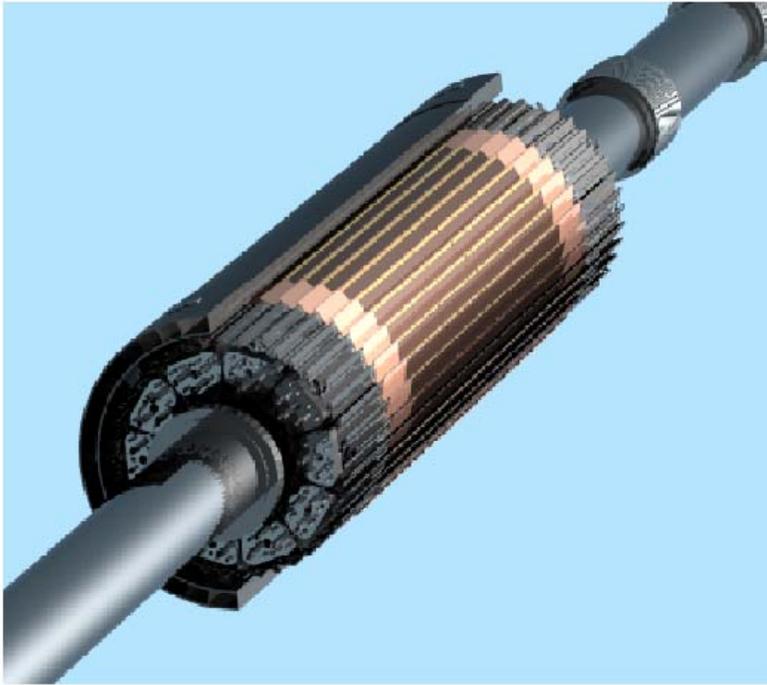
Fig.1a

Fig. 1a   The two innermost silicon layers of the ALICE ITS are shown together with a
portion of the beam pipe. These layers are made by hybrid pixel detectors.
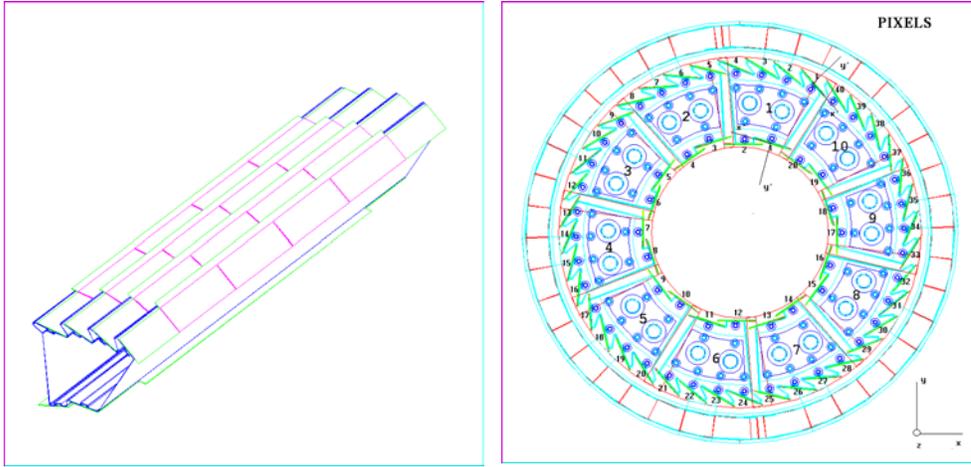
PIXELS

Fig.1b

Fig. 1b   One of the ten sectors in which the two pixel layers are subdivided is shown in the left part of the figure. Each sector is built using two and four tiles, called 'staves', for the inner and outer layer respectively. Each stave is made by four ladders and twenty read-out chips.

The right part of the figure shows a section of the SPD, orthogonal to the Z-axis. The tiles on the outer layer form a larger angle, with respect to the radial direction, compared to the inner layer staves. The end sector cooling system is also shown.

η

Zv (mm)

Fig. 2a

η

Zv (mm)
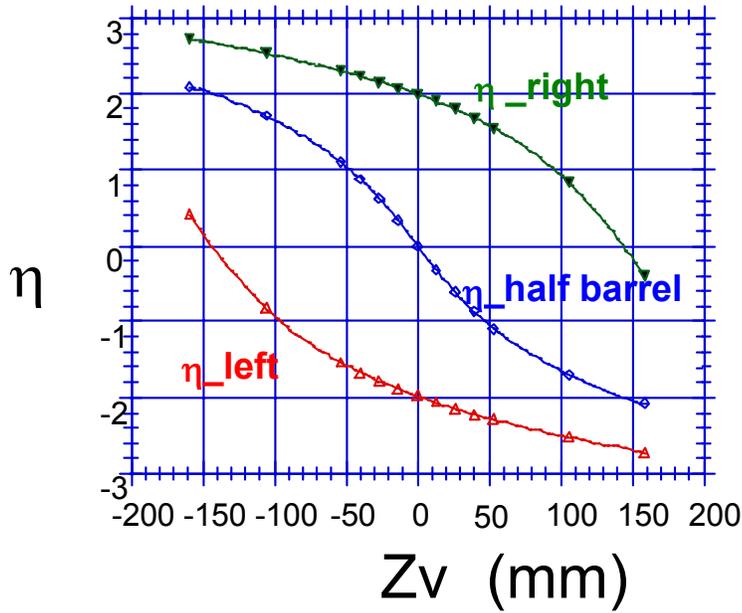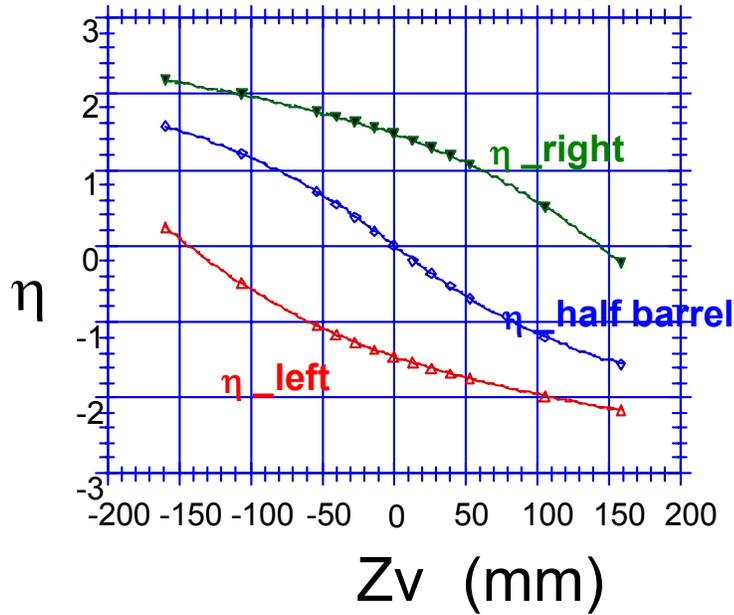
Fig. 2b

Fig. 2a   The pseudo-rapidity (η) coverage range versus the primary interaction vertex position along the beams axis (Z_v) for the inner SPD (layer1 at r=4cm) is shown. The three curves refer to different positions, corresponding to the centre (η_half barrel) and to the ends of the layer (η_left and η_right).

Fig. 2b   The pseudo-rapidity (η) coverage range versus the primary interaction vertex position along the beams axis (Z_v) for the outer SPD (layer2 at r=7cm) is shown. The three curves refer to different positions, corresponding to the centre (η_half barrel) and to the ends of the layer (η_left and η_right).
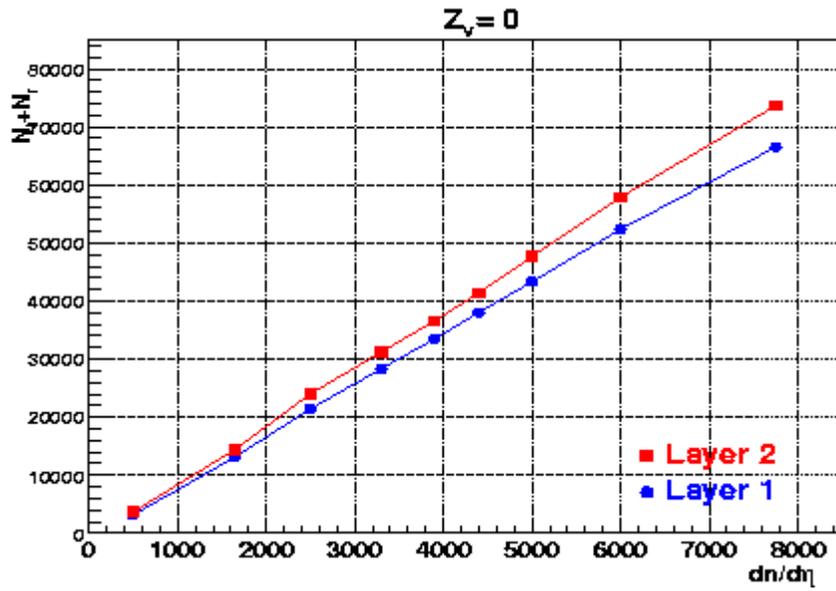
Fig. 3a   Total number of digits in layer 1 (inner SPD) and layer 2 (outer SPD) versus the generated multiplicity, for $Z_v = 0$.
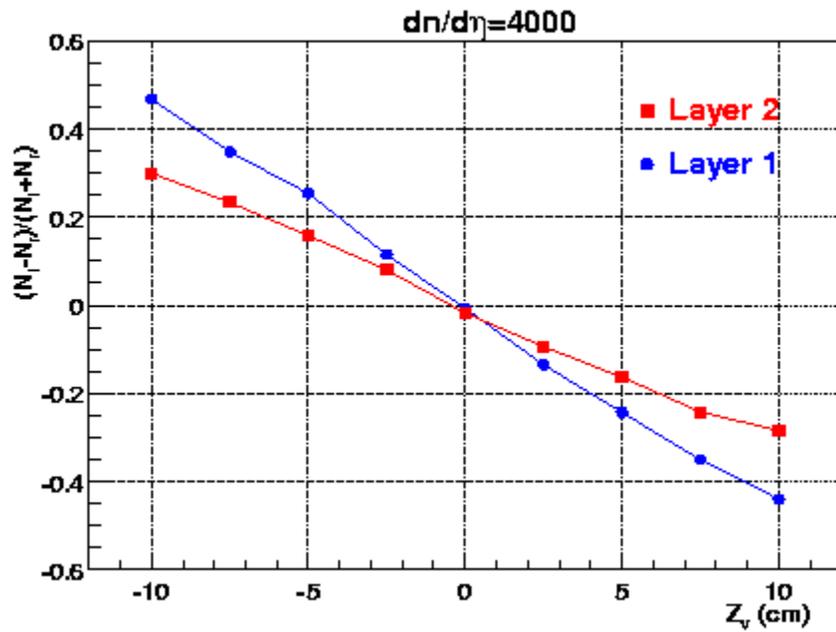
Fig. 3b   Left-right asymmetry in layer 1 (inner SPD) and layer 2 (outer SPD) versus the longitudinal position of the vertex, for $dn/d\eta=4000$.
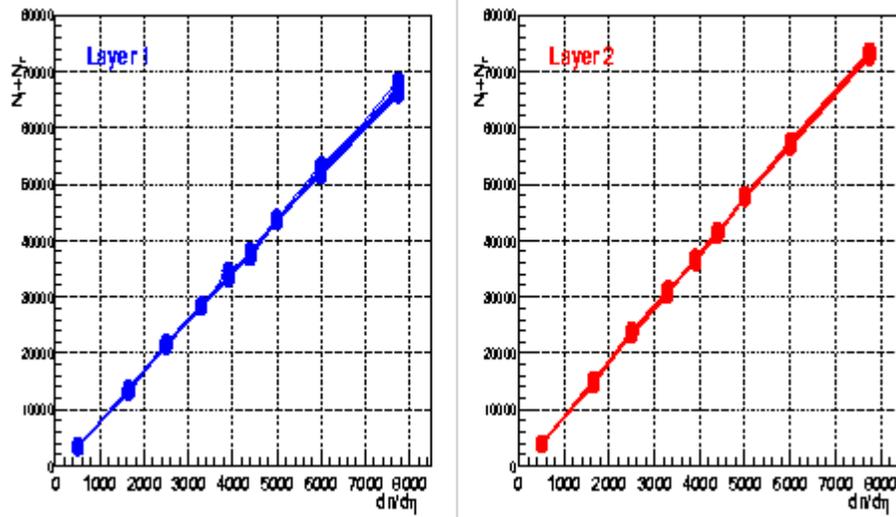
Fig. 4a   Total number of digits in layer 1 (inner SPD) and layer 2 (outer SPD) versus the generated multiplicity, for $Z_v = 0$. For each multiplicity the results from 15 events, generated in the same conditions, are reported.
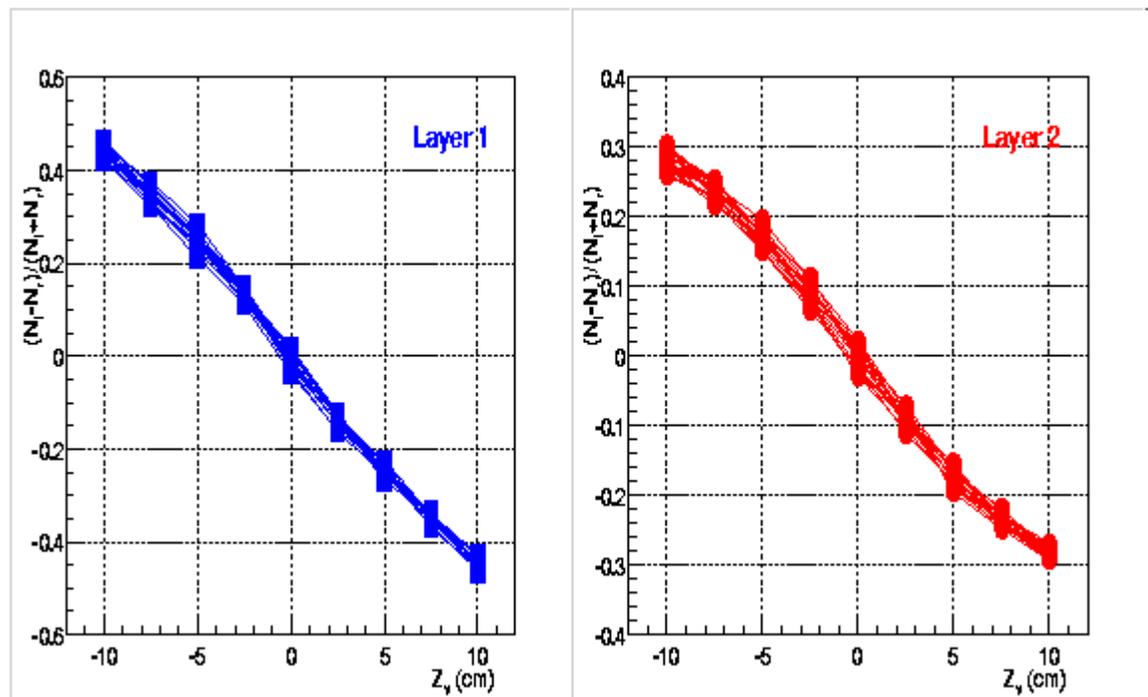
Fig. 4b   Left-right asymmetry in layer 1 (inner SPD) and layer 2 (outer SPD) versus the longitudinal position of the vertex, for $dn/d\eta = 4000$. For each vertex position the results from 15 events, generated in the same conditions, are reported.
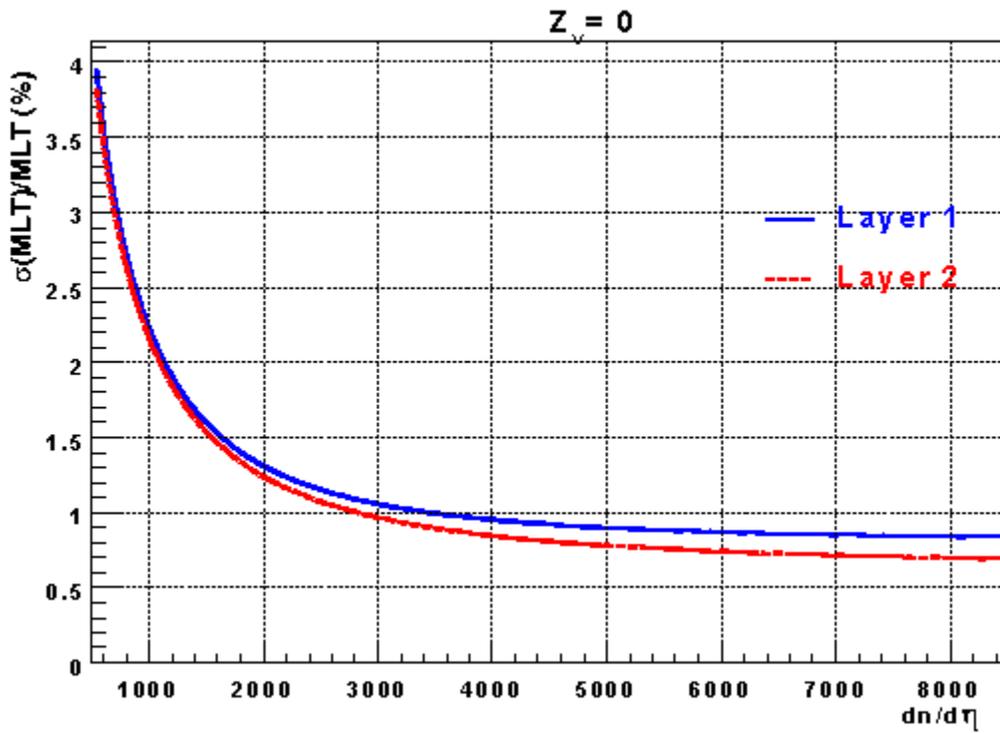
Fig. 5a   Relative error on the true event multiplicity as a function of the generated dn/dη. The higher curve refers to the inner SPD (layer 1) and the lower curve refers to the outer SPD (layer 2). Note the small differences (<2%) between the two curves.
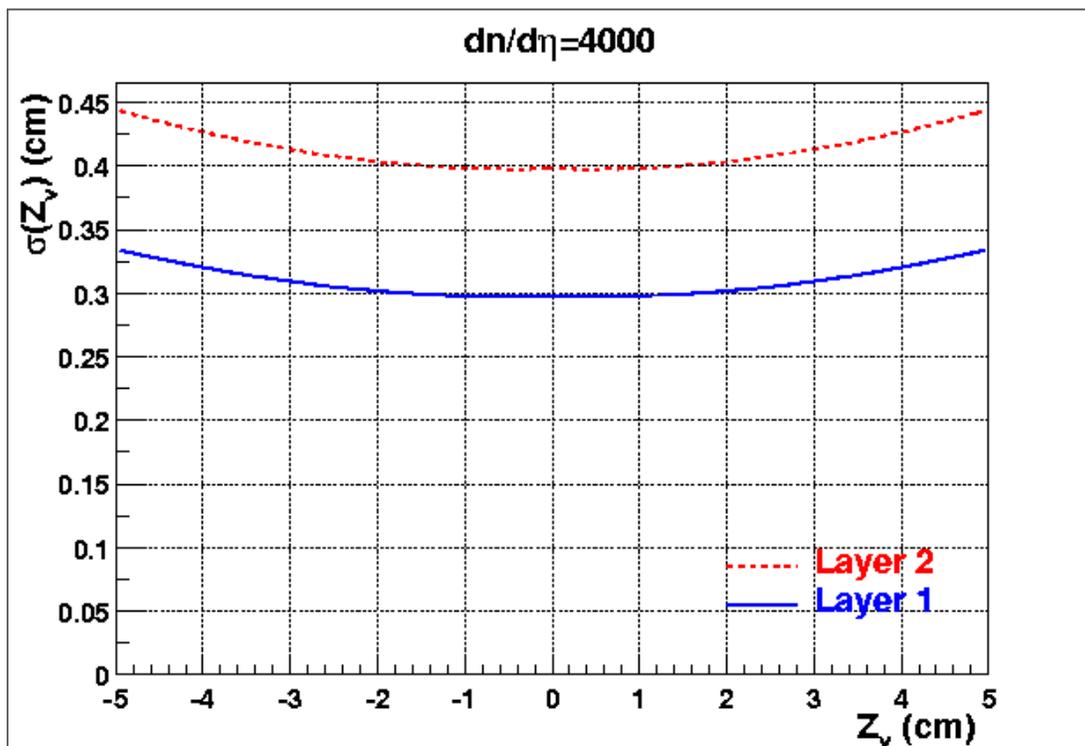
Fig. 5b   Error on the longitudinal position (i.e. along the Z-axis) of the primary vertex as a function of the primary vertex position used in the simulation. The upper curve refers to the outer SPD (Layer 2) and the lower curve refers to the inner SPD (layer 1).
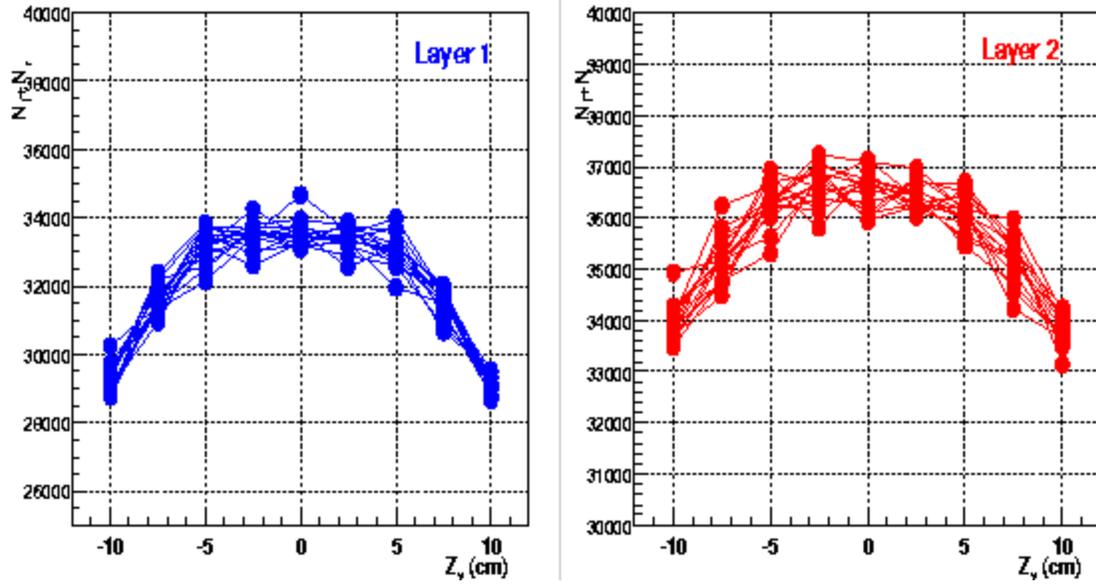
Fig. 6a   Total number of digits in layer 1 (inner SPD) and layer 2 (outer SPD) versus the primary vertex position along the Z-axis (Z_v), for dn/dη=4000. For each vertex position the results from 15 events, generated in the same conditions, are reported.

Fig. 6b   Left-right asymmetry in layer 1 (inner SPD) and layer 2 (outer SPD) versus the generated multiplicity, for Z_v = 0. For each multiplicity the results from 15 events, generated in the same conditions, are reported.